Soft Matter

Accepted Manuscript

ROYAL SOCIETY OF CHEMISTRY

www.rsc.org/softmatter

Exploring the dynamics of phase separation in colloid-polymer mixtures with long range attraction

Juan Sabin,[1,2] Arthur E. Bailey,[3] and Barbara J. Frisken[1,*]

[1]*Department of Physics, Simon Fraser University, Burnaby, British Columbia, Canada, V5A 1S6*

[2]*Biophysics and Interfaces Group, Department of Applied Physics, University of Santiago de Compostela, E-15782 Santiago de Compostela, Spain*[†]

[3]*Scitech Instruments Inc., North Vancouver, British Columbia, Canada, V7J 2S5*

(Dated: April 18, 2016)

Abstract

We have studied the kinetics of phase separation and gel formation in a low-dispersity colloid — non-adsorbing polymer system with long range attraction using small-angle light scattering. This system exhibits two-phase and three-phase coexistence of gas, liquid and crystal phases when the strength of attraction is between 2 and 4 k_BT and gel phases when the strength of attraction is increased. For those samples that undergo macroscopic phase separation, whether to gas-crystal, gas-liquid or gas-liquid-crystal coexistence, we observe dynamic scaling of the structure factor and growth of a characteristic length scale that behaves as expected for phase separation in fluids. In samples that gel, the power law associated with the growth of the dominant length scale is not equal to 1/3, but appears to depend mainly on the strength of attraction, decreasing from 1/3 for samples near the coexistence region to 1/27 at 8 k_BT, over a wide range of colloid and polymer concentrations.

Keywords: colloid-polymer, depletion, phase separation, crystallization, gelation, dynamic scaling, small-angle light scattering, attractive interaction

*Corresponding author: frisken@sfu.ca

[†]Current address: AFFINImeter Scientific & Development Team, Software 4 Science Developments Inc., Santiago de Compostela, Spain

I. INTRODUCTION

Colloidal systems provide a rich playground of equilibrium and non-equilibrium phases in which to explore fundamental problems such as the kinetics of crystallization, the aging of gels, and the nature of glassy states [1]. Time and length scales are easily accessible and interactions between colloidal "atoms" can be precisely tuned. In particular, an attractive interaction can be generated by adding a non-adsorbing polymer to a colloidal dispersion, where the range of the interaction is tuned by changing the ratio q_R of the size of the polymer in the dilute limit to the size of the colloidal particle and the strength of the interaction is set by the polymer concentration [2].

The phase diagram for systems where the range of attraction is short, $q_R < 0.25$, and the strength of the attraction is weak (comparable to k_BT), includes regions of fluid, crystal, coexisting fluid and crystal and, at high colloid concentration, a non-equilibrium repulsive glass. As the strength of the attractive potential is increased, other non-equilibrium phases are observed [3, 4]. At low colloid concentration, fractal clusters form by mechanisms similar to nucleation and growth. At intermediate concentration, transient gels are observed that are characterized by a length scale that evolves to a certain point before the gel collapses or the structure arrests. These structures are attributed to a metastable region of gas-liquid coexistence; samples quenched into this region phase separate into gas and liquid phases by a process similar to spinodal decomposition but the evolution is arrested when the concentration of the liquid phase crosses into the glass phase [5–8]. At high colloid concentration, samples form an attractive glass [9].

Systems with long-range attraction, $q_R > 0.25$, show an even richer phase diagram with colloidal phases demonstrating gas, liquid and crystalline order as well as regions of two-phase (gas-liquid, gas-crystal and liquid-crystal) and three-phase coexistence [10]. Non-equilibrium phases, such as gels, form at stronger attractive potentials [11, 12]. While the possibility of different kinetic regimes has been carefully examined [13, 14], detailed experimental study of the dynamics of formation of equilibrium and non-equilibrium phases is limited to a few studies. It has been shown that fluid-fluid phase separation of polymer-colloid mixtures is consistent with the phase separation of binary mixtures if the particle diameter is used as an estimate of the minimum correlation length [15]. Ageing of gel-forming samples has been investigated by confocal microscopy and rheology in a more disperse emul-

sion system that uses xanthan gum as the depletant at a colloid concentration of 0.2 and $q_R = 0.60$ [12]. Dynamic scaling consistent with spinodal decomposition was observed in the evolution of the structure function prior to arrest. However, the characteristic length scale grew more slowly than the $t^{1/3}$ power law observed in normal fluid phase separation, with the exponent becoming smaller for deeper quenches. A more recent paper from this group [16] compares the dynamics of phase-separating colloid-polymer systems closer to the coexistence curve in three systems with different interaction ranges using confocal microscopy. They identified a crossover between classical phase separation and gelation.

In this work, we present results of small angle light scattering (SALS) experiments for a system characterized by a long-range depletion interaction, $q_R \approx 0.5$. Low dispersity allows for crystallization of the colloid. As a result, the phase diagram includes gas-liquid, gas-crystal and gas-liquid-crystal coexistence regions as well as gel phases at higher strength of attraction. Samples spanning a wide range of colloid and polymer concentration were made, allowing us to investigate kinetics over a more extensive range of environments than previously studied. The results show that the structure evolves by growth of a single characteristic length scale, as described for phase separation [17] but observed more widely. Extending results of Ref. [12], we observe that the growth of the characteristic length scale follows a power law with an exponent that decreases with quench depth. We find that the growth exponent scales with the strength of attraction over a wide range of sample conditions.

II. MATERIALS AND METHODS

A. Sample preparation

The samples consisted of mixtures at various concentrations of colloidal particles and non-adsorbing polymer dispersed in a solvent. The colloids were poly(methylmethacrylate) (PMMA) spheres sterically stabilized by a thin, chemically grafted surface layer of poly-12-hydroxystearic acid [18, 19]. The solvent was a 45:55 mixture (by mass) of cis/trans decahydronaphthalene (decalin) and tetrahydronaphthalene (tetralin), which matches the refractive index of the colloidal particles, reducing both the scattering in the system and the van der Waals attraction between the particles. Because the PMMA particles absorb a small amount of tetralin, the particles were heat-shocked to rapidly reach equilibrium swelling [20].

The radius of the swollen particles was calculated to be (230 $\pm$ 10) nm by correcting the radius of the swollen particles measured by static light scattering by addition of the thickness of the steric layer thickness obtained previously for particles made by this method [20, 21]. The relative dispersity was measured to be 0.06 by static light scattering. The non-adsorbing polymer, polystyrene (PS), had a molecular weight $M_w = 13.2$M g/mol and dispersity index $M_w/M_n = 1.05$ (Polymer Laboratories Ltd., UK). A fit of the Debye relation to the angular dependence of the light scattered by a dilute suspension of the polymer in the decalin:tetralin mixture yielded a radius of gyration of (120 $\pm$ 4) nm, from which we estimate an overlap concentration ${c_p}^* = \left(3M_w\right)/\left(4\pi N_A {R_g}^3\right) = 3.0$ mg/mL and a relative range of the depletion attraction in dilute solution of $q_R = 0.52 \pm 0.03$.

Eight series of samples were prepared for this study. The initial sample in each series was made at high colloid and/or polymer concentrations, and then successively diluted with the solvent mixture to cross the gas-liquid-crystal coexistence region. After each dilution, the new sample was mixed by tumbling in a rotator for 15 minutes before starting any measurements. We defined the time the sample was removed from the rotator as $t = 0$ in all experiments. The initial colloid volume fraction ϕ_c and polymer concentrations c_p of each series (S1-S8) can be found in Table I. To determine the initial colloid volume fraction of each series, the colloid concentration for the initial samples was obtained from a single hard sphere sample whose concentration was obtained from analysis of the phase volumes for samples in the coexistence region [22].

The samples made by diluting each of these initial samples are shown in Fig. 1. This diagram also shows the three-phase region expected for this system calculated using the generalized free volume theory (GFVT) developed by Fleer and Tuinier [23] for $q_R = 0.45$ and assuming theta-solvent for the polymer. This value of q_R provides a good description of our data, although it is slightly lower that the value anticipated from measurement of particle size and polymer radius of gyration. This batch of colloids was slightly more disperse (6% compared to 5%) as measured for previous batches. It has been shown that increased dispersity can affect the phase diagram [24].

TABLE I: Initial colloid volume fraction ϕ_c and polymer concentrations c_p (in units of mg/mL) for the eight series (S1-S8) of colloid-polymer dispersions studied.

Series	ϕ_c	c_p
S1	0.090	1.24
S2	0.129	1.10
S3	0.329	1.55
S4	0.387	1.12
S5	0.466	0.857
S6	0.387	0.512
S7	0.538	0.270
S8	0.539	0.110

B. Small-angle light scattering

We used a custom-built small-angle light scattering (SALS) apparatus to measure light scattered at small angles ranging from 0.08 to 10 degrees [25]. Based on previous work by F. Ferri [26], this instrument uses a CCD camera to image the scattered light in the focal plane of the collection lens. Samples were placed in glass cells having an internal pathlength of 4 mm. Measurements were started within 8 s of the time that the sample was removed from the rotator and images were acquired every 3 s for 30 s, then every 5 s for 100 s, every 30 s for 900 s and finally every 500 s for 15,000 s, after which no further changes were detected. Samples were remixed between runs.

Phase separation of the sample was characterized by the development of a bright ring in the images with a corresponding peak in the intensity data at a scattering wavevector $q_m = (4\pi n/\lambda)\sin(\theta_m/2)$, where n is the refractive index of the solvent, λ is the wavelength of the incident light, and θ_m is the scattering angle at which the maximum intensity occurs. Such a ring signifies a mean spacing between colloid-rich domains of $L_m = 2\pi/q_m$ [27]. To analyze each image, data were corrected by subtracting the scattering from the solvent, as measured in a cell of the same thickness, and azimuthally-averaged at constant scattering angle from the transmitted beam. A Gaussian function was fit to a limited number of points near the peak in the intensity to find the peak value q_m and the maximum intensity $S(q_m)$.

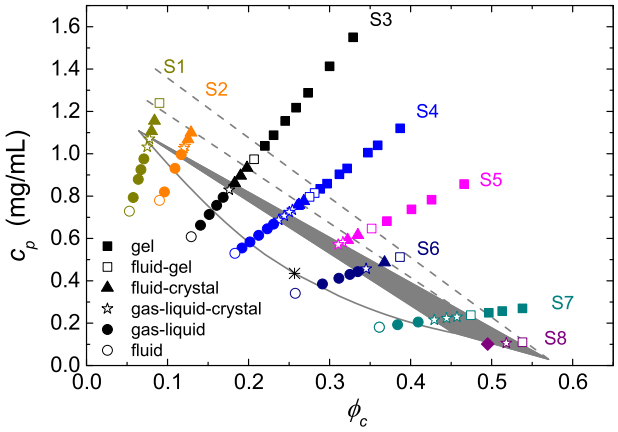

FIG. 1: Phase diagram showing the compositions of the eight series (S1-S8) of samples under study plotted as a function of colloid volume fraction ϕ_c and polymer concentration c_p in the sample. The symbols represent the final state of the system observed at each composition as described in the text: gel, fluid-gel coexistence, fluid-crystal coexistence, gas-liquid-crystal coexistence, gas-liquid coexistence, fluid. The solid grey triangle represents the three-phase coexistence region, the solid grey curve represents the gas-liquid coexistence curve and the black star the critical point as calculated following GFVT [23] assuming the solvent mixture is a theta-solvent for the polymer and that $q_R = 0.45$. The dashed grey lines approximate boundaries between our observations of fluid-crystal, fluid-gel and gel phases and are provided as guides to the eye.

III. RESULTS AND DISCUSSION

A. Visual observations

Visual inspection of the samples shows behavior that depends on the colloid and polymer concentrations of the samples and is consistent with previous results from this system [10]. All samples show an increase in turbidity following homogenization. At low dilution, the intensity fluctuations from the samples become static, which is evidence of an arrested structure. At the lowest dilutions of series S3, S4, S5 and S7, no change in structure was observed over at least two days, the time taken for dilute fluid phases to sediment in this system. After further dilution, i.e. at lower polymer and colloid concentration, structures are formed that sediment after a period of time that becomes shorter as the dilution is increased. This behavior is characteristic of weak colloidal gels [5, 28]. As the dilution is increased further, samples phase separate into gas-crystal, gas-liquid-crystal and gas-liquid

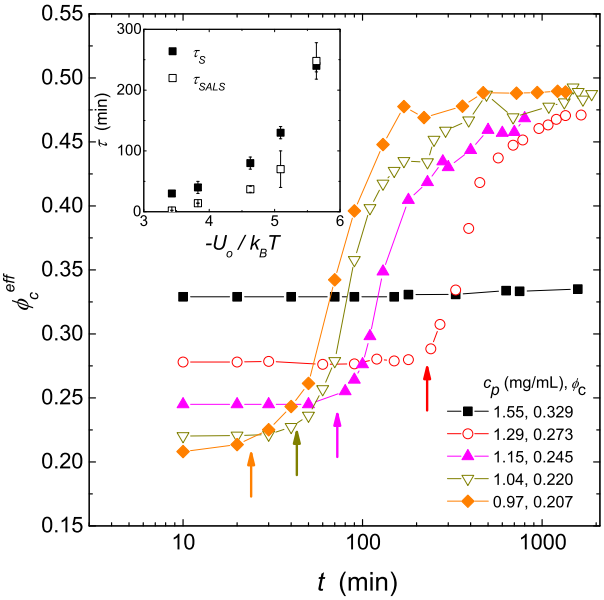

FIG. 2: Temporal evolution of the effective volume fraction of colloid $\phi_c{}^{eff}$ in gel samples from series S3. The sample compositions are shown in the legend. Arrows represent the onset of sedimentation. The inset compares the time when the SALS ring disappears τ_{SALS} (open squares) to the time when sedimentation is observed to begin τ_S (filled squares) as a function of the strength of attraction.

phases. The final structure observed after each dilution is indicated on Fig. 1.

B. Gel sedimentation

We obtained further information about the structure of the gel phase by studying the sedimentation of the samples that gel. We measured the height of the sediment h_g as a function of time following mixing as recorded in photographs taken every 10 minutes after mixing [28]. From the height, we estimated the effective colloid volume fraction $\phi_c{}^{eff}$ of the gel phase from the colloid volume fraction of the sample ϕ_c and the ratio of the total height of the sample h_o and the height of the gel phase

$$\phi_c{}^{eff} = \frac{h_o}{h_g}\,\phi_c \quad . \tag{1}$$

Results for a selection of samples in series S3 are shown in Fig. 2. At the beginning of the experiment, before sedimentation starts, the effective colloid volume fraction is equal to the

sample volume fraction ϕ_c. The sample with highest polymer and colloid concentration, $c_p = 1.55$ mg/mL and $\phi_c = 0.329$, where the data is shown as solid black squares, did not sediment appreciably over two days so ${\phi_c}^{eff}$ remains constant. As the other samples sediment, their effective colloid volume fraction increases reaching a final ${\phi_c}^{eff}$ of 0.5, showing that their final structures are not compact; these results are consistent with observations of other workers [5, 28]. Arrows mark the delay times τ_S when sedimentation starts, as estimated from the curves. The time τ_S increases dramatically as the strength of attraction $-U_o/k_B\,T$ increases, as shown in the figure inset (filled squares). Values of the attractive potential at contact were calculated from GFVT [23]; further details can be found in the Appendix. Recent work [29] reviews the relationship between the delay time and microscopic processes that causes it and presents a model which connects gel collapse to the kinetics of bond breaking.

C. Small-angle light scattering

The evolution of the structure of all samples was monitored by SALS. For most samples, CCD images exhibit a diffuse ring that appears at high q a few seconds after mixing and evolves with time. Characteristic SALS data are shown in Fig. 3 for two samples in series S3 whose equilibrium structures are (a) gel and (b) gas-crystal coexistence. The first measurements after initialization show little structure but exhibit dynamic intensity fluctuations. As time passes, a peak forms in the scattered intensity at high q. It grows in amplitude and moves to smaller q as the time after mixing increases. In the more concentrated sample, Fig. 3a, evolution appears to cease as there is no obvious change in q_m and the peak amplitude. This lack of dynamics and arrest at a final characteristic length scale is characteristic of formation of a gel structure, consistent with observations discussed previously. In most samples with these characteristics, the SALS ring eventually becomes asymmetric, consistent with gravitational collapse [12, 30]. The time when this occurs τ_{SALS} is shown on the inset of Fig. 2 (open squares) and is consistent with sedimentation times τ_S estimated from visual observations. The difference between τ_S and τ_{SALS} indicates that the gels start sinking some minutes after they lose their internal structure. As the sample is diluted and the polymer and colloid concentrations are decreased, the ring collapses more quickly and gel collapse occurs earlier. In samples with lower colloid and polymer concentrations, as

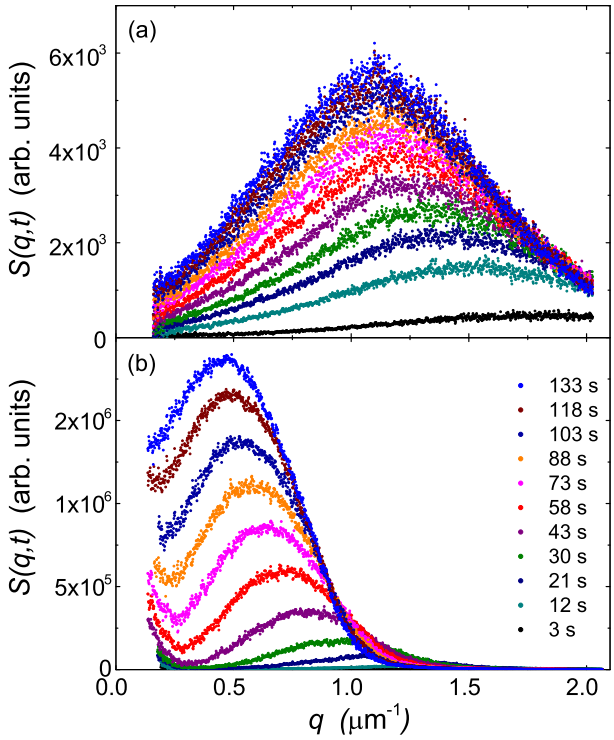

FIG. 3: Temporal evolution of the scattered intensity as a function of scattering vector measured at different times following mixing (3< t <133 s) for two samples from series S3 with (a) $\phi_c = 0.258$ and $c_p = 1.22$ mg/mL (gel) and (b) $\phi_c = 0.198$ and $c_p = 0.93$ mg/mL (gas-crystal coexistence).

shown in Fig. 3b, the peak evolves to the point where it moves to scattering wave-vectors too small to measure and we observe macroscopic phase separation, either into three phases, crystal-liquid-gas, or into two phases, liquid-gas or crystal-gas or crystal-fluid. A peak was not observed in the SALS data for samples from series S8, although macroscopic phase separation was observed. We believe this is because contrast between the phases was particularly low in this series, making it difficult to observe the scattering ring with our instrument.

The scattered intensity $S(q,t)$ obtained for each data set was scaled by normalizing the scattering wavevector by its value where the intensity is maximum q_m and the intensity by the maximum value $S(q_m)$. Remarkably, we find that all data sets collapse when scaled in this way, indicating that the structure evolves with a single characteristic length $L_m = 2\,\pi/q_m$. Figure 4 shows results for four samples in series S3, whose equilibrium structures are (a) a gel, (b) gas-crystal coexistence, (c) gas-liquid-crystal coexistence and (d) gas-liquid coexistence for data taken over a time period from 5 to 50 s after initialization. The scaling of the

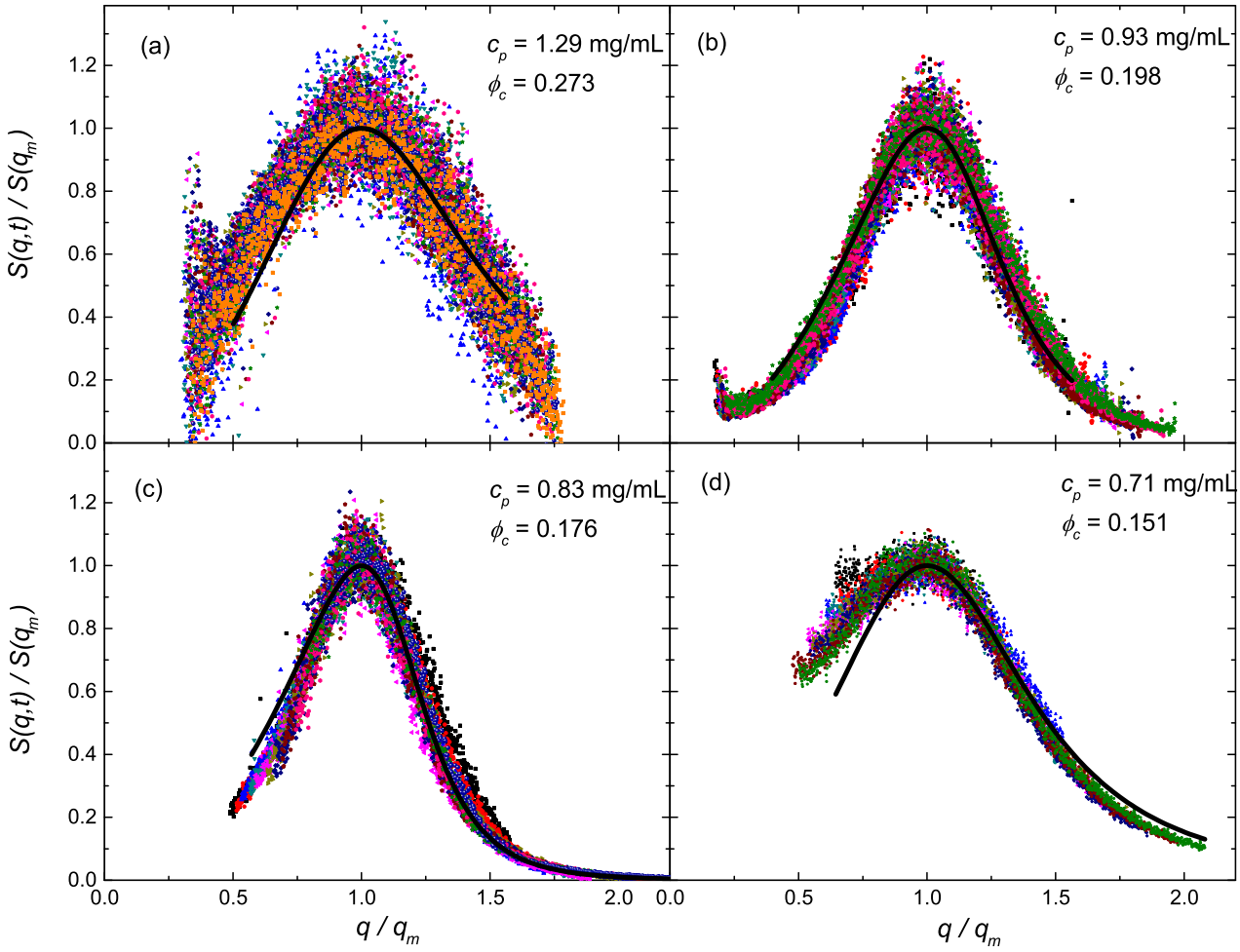

FIG. 4: SALS data with the intensity scaled by the peak intensity plotted as a function of the scattering vector scaled by the peak wavevector for four samples in series S3 (compositions shown on the graph) that evolve to different structures: (a) gel, (b) gas-crystal coexistence, (c) gas-liquid-crystal coexistence, and (d) gas-liquid coexistence. The curves represent the dynamic scaling function proposed by Furukawa for phase separation in critical samples, Eq. 3, with $\gamma = 3.9$, 6.7, 8.9, and 4.3, respectively, where the uncertainty in γ is 0.3.

evolving data worked well over a period of time — typically for $5 < t < 50$ s, except for the highly concentrated gels where early time data is noisy. In these cases, scaling applied for $75 < t < 130$ s. After this time — i.e. a minute or two — the data does not scale as well, presumably because sedimentation is affecting the structure.

From Fig. 4 we see that the shape of the scaled scattered intensity $F\left(q/q_m\right)$

$$F\left(q/q_m\right) = \frac{S(q,t)}{S(q_m)} \quad , \tag{2}$$

varies with sample composition. H. Furukawa proposed a model function for scaling structure functions that describes both large- and small-q behavior [17]:

$$F\left(q/q_m\right) = \frac{\left(1+\frac{\gamma}{2}\right)\left(\frac{q}{q_m}\right)^2}{\frac{\gamma}{2}+\left(\frac{q}{q_m}\right)^{2+\gamma}} \quad , \tag{3}$$

where γ is the scaling exponent. This function was developed to describe phase separation in binary mixtures but has been applied to many systems. The exponent γ describes structure at small length scales, particularly domain interfaces. We fit this model function to our data; results are shown in Fig. 4 as black curves. We found some deviations for some data sets at either small or large q but it is possible to estimate a value for γ for each data set. There are several experimental limitations that affect the data. In particular, double scattering due to high contrast between colloid and solvent or high background scattering due to low contrast results in small changes in the shape of the scaled data.

The scaling exponent γ is related to the dimensionality of the system. Typically two types of quenches are described: quenches into the region of the phase diagram close to the critical point and off-critical quenches into the metastable region between the binodal and spinodal curves. For critical quenches, where the domains are entangled, Furukawa [17] predicts that $\gamma = 2\ d$, while for off-critical quenches, below the percolation threshold, the prediction is that $\gamma = d + 1$, where d is the dimensionality of the structure. In colloidal gelation, d is interpreted as the fractal dimension [31].

Figure 5 (a) shows the scaling exponent obtained by fitting Eq. 3 to the scaled scattering data. The composition of each sample is shown by placing a marker on the coexistence curve from Fig. 1; the value of γ is represented by the color of the marker. In general the results for γ are consistent with Furukawa's predictions: in the central part of the coexistence region, γ is about 6; near the low ϕ_c corner where we expect phase separation by nucleation γ is about 4; at high c_p where we expect a fractal gel ($d \approx 2$ [31]) the exponent is also 4. However there is a region close to the critical point where the exponent is higher than expected, closer to 8 than 6, and the boundaries between these regions are not sharp. There are some limitations in our determination of γ, however consideration of the results in the

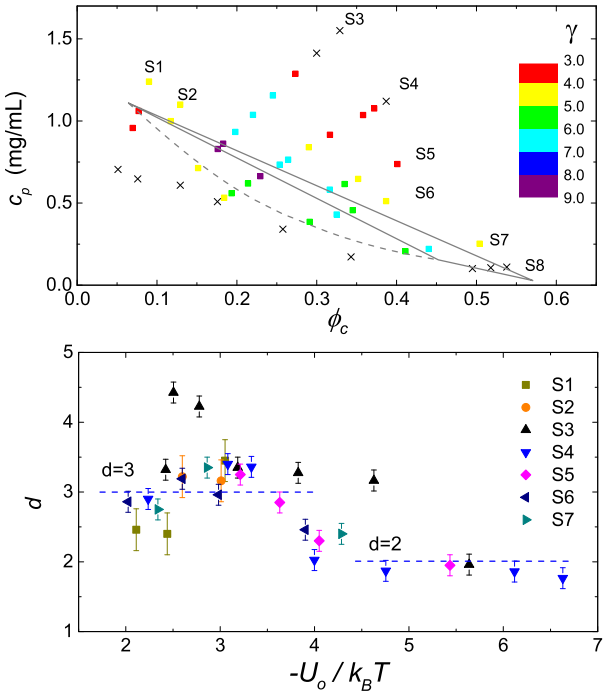

FIG. 5: The scaling exponent for the dynamic structure factor as obtained by fitting Eq. 3 to the SALS data for samples corresponding to those shown in Fig. 1. In part (a), the value of the exponent is depicted by the color of the symbol, as shown in the legend. The samples represented by crosses did not show a spinodal ring. Low c_p, ϕ_c concentration samples did not phase separate but remained homogeneous. Samples at the extreme liquid-crystal end of the three-phase region had very low contrast, precluding any observation of a change in structure. We believe no spinodal ring was observed in the highest concentration samples in series S3 and S4 (gels) because it developed at q larger that we had access to in our SALS instrument. The solid black lines delineate the three-phase coexistence region and the dashed line the gas-liquid coexistence curve as shown in Fig. 1. Part (b) shows the value for d calculated from γ, as described in the text. The dashed lines showing $d = 3$ and $d = 2$ are included as guides to the eye. Values are for samples from series S1-S7, with markers as shown in the legend.

context of the strength of attraction do present a consistent picture. Figure 5 (b) shows value for the dimensionality d calculated from γ as follows. For samples with $\phi_c > 1/6$, we assumed $\gamma = 2d$. For samples below the percolation threshold at $\phi_c = 1/6$, we assumed $\gamma = d + 1$. Results are plotted as a function of the strength of attraction and the error bars are calculated from estimates of the uncertainty in γ for each measurement. For the

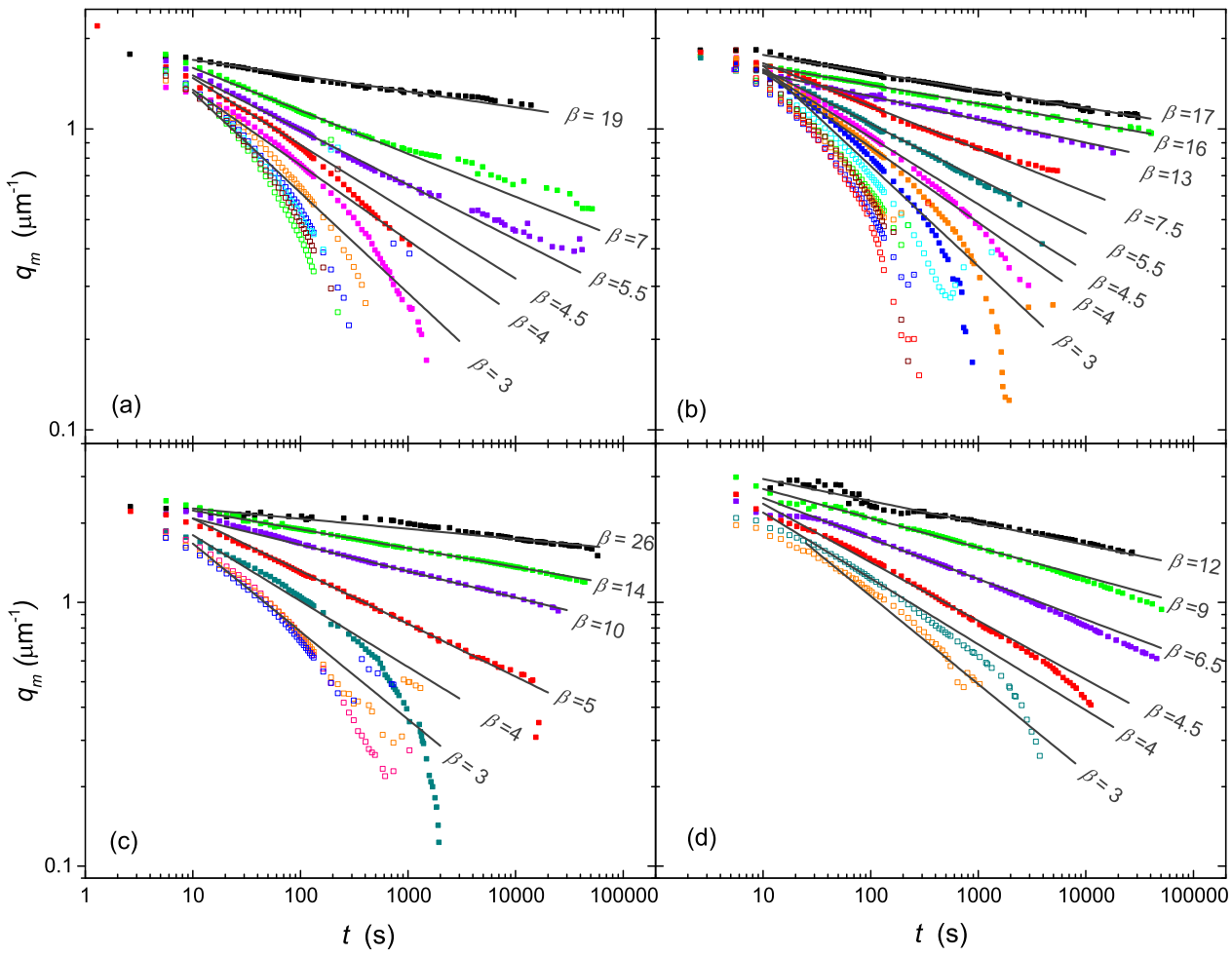

FIG. 6: The change in the peak position with time for samples in series (a) S3, (b) S4, (c) S5 and (d) S7, where each set of data markers corresponds to the temporal evolution of a sample of different colloid and polymer concentration; the compositions of the different samples studied are shown in Fig. 1. The samples that evolve most slowly have the highest colloid and polymer concentration. Open symbols are used for samples that undergo macroscopic phase separation to either gas-liquid, gas-liquid-crystal or gas-crystal phases. Closed symbols are used for samples that form a gel. Lines are used as guides to the eye showing power laws with different exponents.

wide range of colloid concentration and strength of attraction studied here, the results are consistent with $d = 3$ for $|U_o| < 4\ k_B\ T$ and $d = 2$ for $|U_o| < 4\ k_B\ T$. All samples that undergo macroscopic phase separation are consistent with Furukawas scaling function for $d = 3$. This is expected for samples undergoing spinodal decomposition to coexisting liquid and gas phases; note here that samples that evolve to coexisting gas-crystal and gas-liquid-

crystal also follow this scaling. The data for samples that evolve to a gel are consistent with the scaling function for $d \approx 2$, a typical value for fractal aggregates [31].

Figure 6 shows the temporal evolution of the scattering wavevector q_m at which the intensity is maximum for samples in series S3, S4, S5 and S7. Evolution of the characteristic length scale L_m is evident even in the highest concentration sample in each series. As the samples are diluted, L_m grows more quickly. The growth of L_m shows power-law behavior, $L_m \propto t^{1/\beta}$; the lines on each graph show different β values. The samples shown with solid symbols form gels. There are two groups: at higher concentration samples grow with a single power law until evolution is interrupted by sedimentation. At slightly lower concentrations β decreases before sedimentation. The samples shown with open symbols show macroscopic phase separation; in these samples, L_m grows with a power law of 1/3, or $\beta = 3$, at early times.

Growth of the characteristic length scale with a power law of 1/3 is expected for phase separation of a binary mixture, and has been observed in liquid-gas phase separation in the polymer-colloid system [15]. Here we see that this behavior is characteristic of all samples that undergo macroscopic phase separation. In fact, the evolution of the position of the peak in the structure factor for samples that undergo macroscopic phase separation is remarkably similar regardless of whether the final state is gas-crystal, gas-liquid-crystal or gas-liquid coexistence, as can be seen by comparing data with open symbols in Fig. 6.

When scaled, the data agree quantitatively with the scaling prediction proposed by Furukawa [17]. For example, in Fig. 7 we compare data for samples from series S1-S7 that show gas-liquid-crystal coexistence in equilibrium. In this figure, the time has been scaled by the Brownian diffusion time τ_B and the peak position has been scaled by the particle diameter a. The data show good agreement with the empirical expression proposed by Furukawa for phase separation in systems with a conserved order parameter (shown as a solid curve in Fig. 7), which is consistent with predictions for an initial $t^{-1/3}$ power law dependence typical for diffusion-limited growth and a t^{-1} dependence at longer times due to growth dominated by surface tension. At $t/\tau_B \approx 100$, when the spacing between phase-separated regions is approximately equal to the capillary length $L_c = \sqrt{\gamma/g\Delta\rho}$ [41], the rings begin to collapse faster than the Furukawa prediction, consistent with sedimentation. The crosses show data from recent experiments carried out at the International Space Station using a similar colloid-polymer mixture in a similar region of the phase diagram. In microgravity,

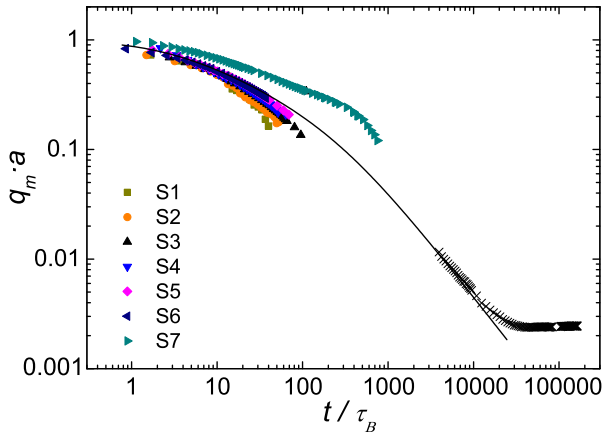

FIG. 7: Time-dependence of the peak position $q_m(t)$ for the first sample in the three-phase region for samples from series S1-S7. The time is normalized by the Brownian diffusion time $\tau_B = \frac{6\pi\eta a^3}{k_B T}$, where η is the viscosity of the polymer solution in the free volume, which is calculated by taking both the concentration of polymer, using the Mark-Houwink-Sakurada equation [32], and the colloid volume fraction [33] into account, using a solvent viscosity of 2.165 mPa·s. The peak position $q_m(t)$ is normalized by the particle diameter a. Data from Ref. [34], shown as crosses, show long time evolution observed in a microgravity environment. The curve shows the expression proposed by Furukawa for binary fluids in absence of gravity capturing the early ($L_m \sim t^{1/3}$) and late time ($L_m \sim t$) scaling behavior.

phase separation does follow the t^{-1} dependence at longer times, before becoming arrested by the formation of crystals in the liquid phase [34].

The samples shown as solid symbols in Fig. 6 form gels. The characteristic length scale of the gels also grows algebraically, although more slowly than usually seen during phase separation. This behavior appears to start very early in the evolution of the phases; i.e. there does not appear to be a period where growth follows a $t^{-1/3}$ power law before rolling over into a new exponent. Figure 8 shows the inverse of the growth exponent β for samples from series S1-S7 plotted (a) as a function of the colloid volume fraction and (b) as a function of the strength of the attractive potential at contact, calculated from GFVT [23] (further details can be found in the Appendix). Figure 8(a) demonstrates that, while β increases with ϕ_c for all series, there are other factors influencing the size of β. Figure 8(b) shows the importance of the strength of the attractive potential. Most of the data collapse when plotted as a function of the strength of the attractive interaction, showing the growth is

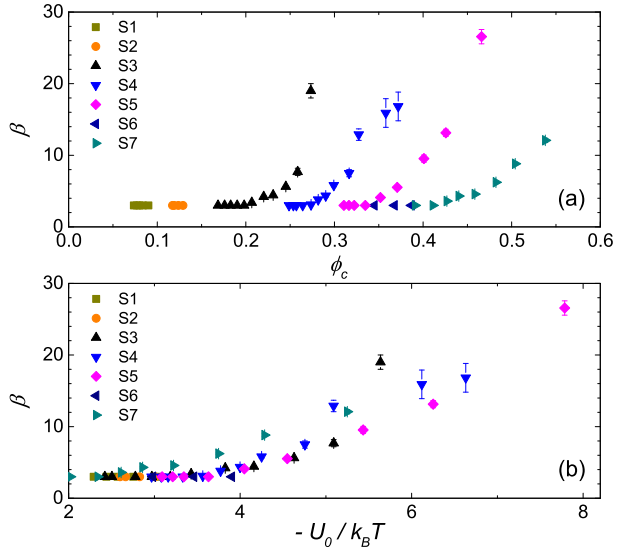

FIG. 8: Inverse of the growth exponent as a function of (a) colloid volume fraction and (b) strength of the attractive interaction for samples from series S1 through S7. At small interaction potential, the growth exponent is approximately 1/3 at early times. When the strength of attraction is greater than $|U_o| \sim 4k_BT$ it decreases. The growth exponent appears to be largely determined by the strength of attraction at contact.

controlled in large part by the strength of the attraction and appears to be independent of ϕ_c. For samples with $-2 < U_o - 4\ k_BT$, $\beta = 3$. These samples exhibit macroscopic phase separation. When the strength of attraction exceeds 4 k_BT, β increases. In these samples, macroscopic phase separation is not observed and gel formation occurs consistent with other work [8, 12, 35]. Samples with $-4 > U_o > -5.5\ k_BT$ correspond to those in Fig. 6 where sedimentation is proceeded by an increase in β, while samples with $-5.5\ k_BT > U_o$ correspond to those where the growth exponent is constant until the gel collapses. Series S7 has the highest overall colloid volume fraction and the fact that the data for this series lie above the data for the other series indicates that, at high enough colloid concentration, crowding does impact the behavior, further slowing the temporal evolution of the gel.

Recent results for an emulsion-based colloidal system with long range attraction [12, 16] also showed a strong dependence of the exponent on the strength of attraction. The experiment studied a series of samples having the same colloid volume fraction but different polymer concentrations resulting in a range of potentials $-5 > U_o > -9\ k_BT$. Our results extend these results to a wider range of experimental conditions, in particular a wider range

of colloid concentration.

Slow phase separation dynamics has been attributed to differences in viscoelastic properties of the separating phases as described in theories of viscoelastic phase separation [36]. Simulations of a binary Lennard-Jones mixture with glass-forming properties show phase separation that becomes slower and slower as the system is quenched more deeply into the two-phase region [37, 38], evolving from surface-tension driven diffusive motion at high temperature to spatially-heterogenous thermally-activated motion at low temperature. While this picture does appear to be a good match to the colloid-polymer system, these simulations show logarithmic, rather than algebraic, growth of the characteristic length scale.

IV. SUMMARY AND CONCLUSIONS

In summary, we have studied macroscopic phase separation and gelation in a colloid-polymer system with long range attraction and low dispersity. We have varied the polymer and colloidal concentration by diluting a series of high concentration samples in order to cross through the phase diagram, exploring gels, gas-crystal coexistence, gas-liquid-crystal coexistence and gas-liquid coexistence using direct visualization and SALS. All samples show a peak in the scattered intensity that grows and moves to smaller scattering wave vector with time. In samples that macroscopically phase separate, the peak continues to grow and to move to smaller and smaller q until it can no longer be measured in our SALS apparatus.

The scattering data for samples in all series except the series with highest colloid concentration and lowest polymer concentration (S8), where contrast was too low to allow adequate measurement, can be represented by a universal curve that depends only on the ratio q/q_m. The scaling exponent associated with high-q scattering depends on sample composition, with samples that show macroscopic phase separation in the centre of the phase diagram being characterized by a scaling parameter consistent with spinodal decomposition. When interpreted in terms of the dimensionality d, the scaling behavior is consistent with $d = 3$ for samples with weaker attraction that macroscopically phase separate ($< 4k_B\,T$), and $d = 2$ for samples that gel, which have stronger attraction ($> 4k_B\,T$).

The characteristic length scale evolves with a power law of exponent $1/\beta$. Independent of the final state, all samples that exhibit macroscopic phase coexistence show features of initial phase separation driven by classical spinodal decomposition: the position of the SALS ring

collapses with a power law of exponent 1/3. In samples that form gels, the domain spacing decreases from 1/3 to 1/27 as the polymer concentration is increased. Remarkably, the dynamics appear to depend mainly on the strength of the attractive interaction across a wide range of colloid concentrations.

Acknowledgments

This research was supported by the Canadian Space Agency and by the Natural Science and Engineering Research Council of Canada. We are grateful to Mr. David Lee for his assistance in use of the SALS apparatus.

[1] W. C. K. Poon, *Science*, 2004, **304**, 830–831.

[2] W. C. K. Poon, *J. Phys: Condens. Matter*, 2002, **14**, R859–R880.

[3] W. C. K. Poon, A. D. Pirie and P. N. Pusey, *Faraday Discuss.*, 1995, **101**, 65–76.

[4] E. H. A. de Hoog, W. K. Kegel, A. van Blaaderen and H. N. W. Lekkerkerker, *Phys. Rev. E*, 2001, **64**, 021407.

[5] N. A. M. Verhaegh, D. Asnaghi, H. N. W. Lekkerkerker, M. Giglio and L. Cipelletti, *Physica A*, 1997, **242**, 104–118.

[6] L. Starrs, W. C. K. Poon, D. J. Hibberd and M. M. Robins, *J. Phys.: Condens. Matter*, 2002, **14**, 2485–2505.

[7] F. Cardinaux, T. Gibaud, A. Stradner and P. Schurtenberger, *Phys. Rev. Lett.*, 2007, **99**, 118301.

[8] P. J. Lu, E. Zaccarelli, F. Ciulla, A. B. Schofield, F. Sciortino and D. A. Weitz, *Nature*, 2008, **453**, 499–504.

[9] K. N. Pham, A. M. Puertas, J. Bergenholtz, S. U. Egelhaaf, A. Moussaid, P. N. Pusey, A. B. Schofield, M. E. Cates, M. Fuchs and W. C. K. Poon, *Science*, 2002, **296**, 104–106.

[10] S. M. Ilett, A. Orrock, W. C. K. Poon and P. N. Pusey, *Phys. Rev. E*, 1995, **51**, 1344–1352.

[11] J. C. Conrad, H. M. Wyss, V. Trappe, S. Manley, K. Miyazaki, L. J. Kaufman, A. B. Schofield, D. R. Reichman and D. A. Weitz, *J. Rheol.*, 2010, **54**, 421–438.

[12] L. J. Teece, M. A. Faers and P. Bartlett, *Soft Matter*, 2011, **7**, 1341–1351.

[13] F. Renth, W. C. K. Poon and R. M. L. Evans, *Phys. Rev. Lett.*, 2001, **64**, 031402.

[14] R. M. L. Evans, W. C. K. Poon and F. Renth, *Phys. Rev. E*, 2001, **64**, 031403.

[15] A. E. Bailey, W. C. K. Poon, R. J. Christianson, A. B. Scholfield, U. Gasser, V. Prasad, S. Manley, P. N. Segre, L. Cipelletti, W. V. Meyer, M. P. Doherty, S. Sankaran, A. L. Jankovsky, W. L. Shiley, J. P. Bowen, J. C. Eggers, C. Kurta, J. T. Lorik, P. N. Pusey and D. A. Weitz, *Phys. Rev. Lett.*, 2007, **99**, 205701.

[16] I. Zhang, C. P. Royall, M. A. Faers and P. Bartlett, *Soft Matter*, 2013, **9**, 2076–2084.

[17] H. Furukawa, *Adv. in Phys.*, 1985, **34**, 703–750.

[18] L. Antl, J. W. Goodwin, R. D. Hill, R. H. Ottewill, S. M. Owens and S. Papworth, *Colloid. Surface.*, 1986, **17**, 67–78.

[19] M. T. Elsesser and A. D. Hollingsworth, *Langmuir*, 2010, **26**, 17989–17996.

[20] S. E. Phan, W. B. Russel, Z. Cheng, J. Zhu, P. M. Chaikin, J. H. Dunsmuir and R. H. Ottewill, *Phys. Rev. E*, 1996, **54**, 6633–6645.

[21] W. C. K. Poon, E. R. Weeks and C. P. Royall, *Soft Matter*, 2012, **8**, 21–30.

[22] Z. Cheng, P. M. Chaikin, W. B. Russel, W. V. Meyer, J. Zhu, R. B. Rogers and R. H. Ottewill, *Mater. Des.*, 2001, **22**, 529–534.

[23] G. J. Fleer and R. Tuinier, *Adv. Coll. Int. Sci.*, 2008, **143**, 1–47.

[24] S. M. Liddle, T. Narayanan and W. C. K. Poon, *J. Phys.: Condens. Matter*, 2011, **23**, 194116.

[25] D. Lee, I. A. Gutowski, A. E. Bailey, L. Rubatat, J. R. de Bruyn and B. J. Frisken, *Phys. Rev. E*, 2011, **83**, 031401.

[26] F. Ferri, *Rev. Sci. Inst.*, 1997, **68**, 2265–2274.

[27] P. Guenoun, R. Gastaud, F. Perrot and D. Beysens, *Phys. Rev. A*, 1987, **36**, 4876–4890.

[28] W. C. K. Poon and M. D. Haw, *Adv. Coll. Int. Sci.*, 1997, **73**, 71–126.

[29] L. J. Teece, J. M. Hart, K. Y. N. Hsu, S. Gilligan, M. A. Faers and P. Bartlett, *Colloid Surface A*, 2014, **458**, 126–133.

[30] N. A. M. Verhaegh, J. S. van Duijneveldt, J. K. G. Dhont and H. N. W. Lekkerkerker, *Physica A*, 1996, **230**, 409–436.

[31] W. C. K. Poon, L. Starrs, S. P. Meeker, A. Moussa'id, R. M. L. Evans, P. N. Pusey and M. M. Robins, *Faraday Discuss.*, 1999, **112**, 143–154.

[32] H. L. Wagner, *J. Phys. Chem. Ref. Data*, 1985, **14**, 1101–1106.

[33] P. N. Segre, O. P. Behrend and P. N. Pusey, *Phys. Rev. E.*, 1995, **52**, 5070–5083.

[34] J. Sabin, A. E. Bailey, G. Espinosa and B. J. Frisken, *Phys. Rev. Lett.*, 2012, **109**, 195701.

[35] D. G. A. L. Aarts, R. P. A. Dullens and H. N. W. Lekkerkerker, *New J. Phys.*, 2005, **7**, 40.

[36] H. Tanaka, *J. Phys.: Condens. Matter*, 2000, **12**, R207–R264.

[37] V. Testard, L. Berthier and W. Kob, *Phys. Rev. Lett.*, 2011, **106**, 125702.

[38] V. Testard, L. Berthier and W. Kob, *J. Chem. Phys*, 2014, **140**, 164502.

[39] E. D. Siggia, *Phys. Rev. A*, 1979, **20**, 595–605.

[40] G. C. Berry, *J. Chem. Phys.*, 1966, **44**, 4550–4564.

[41] We expect sedimentation to accelerate the phase separation process when the length scale exceeds the capillary length $L_c = \sqrt{\gamma/g\Delta\rho}$ [39], the length of an interface between two fluids that is gravitationally unstable, where γ is the interfacial tension and $\Delta\rho$ is the density difference. For our experiments, we estimate the surface tension from $\gamma = \phi_c U_o/a^2$ [15], where $U_o = -3.5\ k_BT$ is the interaction potential as calculated following Fleer and Tuinier [23], and the difference between the density of PMMA ρ_{PMMA} and the decalin-tetralin mixture ρ_s from $\Delta\rho \approx \phi_c\ (\rho_{PMMA} - \rho_s) = 120$ kg m^{-3}, where we have assumed a colloid concentration of approximately zero in the colloid-poor phase and $\phi_c \approx 0.5$ in the colloid-rich phase. Using these values, we obtain an estimate $L_c = 5\ \mu$m, consistent with the departure from the Furukawa form observed at $t/\tau_B \approx 100$ in Fig. 7.

APPENDIX: CALCULATING THE INTERACTION POTENTIAL

We have calculated the polymer concentration in the free volume and the interaction potential at contact using the generalized free volume theory (GVFT) developed by Fleer and Tuinier for systems consisting of colloid and non-adsorbing polymer, which takes into account the dependence of the depletion thickness on polymer concentration and the effects of polymer non-ideality on the osmotic pressure [23]. We have used the mean field version of the equations as the theta solvent limit is more appropriate for the decalin-tetralin system [40].

The energy of the attractive interaction at contact U_o can be calculated by integration of the following expression derived from Gibb's Law [Eq. 7.11 in Ref. [23]]

$$-\frac{U_o}{k_B\ T} \ = \ \int_0^{\Pi} v_{ov}\ d\Pi \ = \ \int_0^{y} \ (v_{ov}/v) \ \ (d\Pi\ v/dy) \ dy \tag{A.1}$$

where v_{ov} is the overlap volume of two depletion layers in contact, $v = 4\pi a^3/3$ is the colloid volume, Π is the osmotic pressure of the external reservoir and y is the polymer concentration in the free volume ${c_p}^r$ normalized by the polymer overlap concentration ${c_p}^*$. The terms in the integrand can be written [Eqs. 7.10 and 6.12 in Ref. [23]]

$$v_{ov}/v \ = \ q^2\ (q_D + 3/2) \quad , \tag{A.2}$$

$$d\Pi\ v/dy \ = \ {q_R}^{-3} \ \left[1 + 12.3\ y^2\right] \quad , \tag{A.3}$$

where $q_D = \delta/a$ is the relative thickness of the depletion zone of thickness δ around a sphere of radius a, q_R is the relative thickness in the dilute limit, T is the temperature and k_B is Boltzman's constant. The relative thickness of the depletion zone shrinks as the polymer concentration increases because the polymer blob size decreases with concentration. The dependence of the relative thickness of the depletion zone on the polymer concentration in the free volume is given by [Eq. 6.17 in Ref. [23]]

$$q_D = 0.938\ {q_R}^{0.9}\ (1\ +\ 6.02\ y^2\ )^{-0.45} \quad , \tag{A.4}$$

where

$$y = \frac{{c_p}^r}{{c_p}^*} = \frac{c_p}{{c_p}^*\alpha} \tag{A.5}$$

and α is the free volume fraction, given by

$$\alpha = (1 - \phi_c) \ \ \exp\left(-Af - Bf^2 - Cf^3\right) \tag{A.6}$$

with $f = \phi_c/(1-\phi_c)$, $A = (1+q_D)^3$, $B = 3\ {q_D}^2\ (q_D + 3/2)$, and $C = 3\ {q_D}^3$. Since $y = y(\alpha)$, $\alpha = \alpha(q_D)$, and $q_D = q_D(y)$, we started with our experimental parameters, c_p and ϕ_c, and iterated through these equations until the results for q_D and α were consistent and then integrated Eq. A.1 numerically to find the value of the interaction potential for each sample.

Dynamic scaling and growth of structure in colloid-polymer samples spanning the phase diagram depends primarily on the strength of attraction